Preprint
UCRL-JC-142032

Development of Lower Energy Neutron Spectroscopy for Areal Density Measurement in Implosion Experiment at NIF and OMEGA

N. Izumi, R. A. Lerche, T. W. Phillips, G. J. Schmid, M.J. Moran, T. C. Sangster

This article was submitted to
Society of Photo-Optical Instrumentation Engineers 46th Annual Meeting, San Diego, California USA, July 29 - August 3, 2001

August 2, 2001

U.S. Department of Energy
Lawrence Livermore National Laboratory

Development of lower energy neutron spectroscopy for areal density measurement in implosion experiment at NIF and OMEGA

N. Izumi, R. A. Lerche, T. W. Phillips, G. J. Schmid, M.J. Moran, T. C. Sangster

Lawrence Livermore National Laboratory, Livermore, CA 94550

ABSTRACT

Areal density (ρR) is a fundamental parameter that characterizes the performance of an ICF implosion. For high areal densities (ρR> 0.1 g/cm^2), which will be realized in implosion experiments at NIF and LMJ, the target areal density exceeds the stopping range of charged particles and measurements with charged particle spectroscopy will be difficult. In this region, an areal density measurement method using down shifted neutron counting is a promising alternative. The probability of neutron scattering in the imploded plasma is proportional to the areal density of the plasma. The spectrum of neutrons scattered by the specific target nucleus has a characteristic low energy cut off. This enables separate, simultaneous measurements of fuel and pusher ρRs. To apply this concept in implosion experiments, the detector should have extremely large dynamic range. Sufficient signal output for low energy neutrons is also required. A lithium-glass scintillation-fiber plate (LG-SCIFI) is a promising candidate for this application. In this paper we propose a novel technique based on downshifted neutron measurements with a lithium-glass scintillation-fiber plate. The details of instrumentation and background estimation with Monte Carlo calculation are reported.

Keywords: ICF, areal density measurement, down shifted neutron, SCIFI

1. PRINCIPLE OF MEASUREMENT

In a deuterium filled target, the primary reactions are,

$$\begin{aligned} D + D &\rightarrow {}^3He(0.82MeV) + n(2.45MeV) \\ D + D &\rightarrow T(1.01MeV) + p(3.02MeV) \end{aligned} \quad . \tag{1}$$

A fraction of primary neutrons is scattered by the target nuclei in the fuel plasma.

$$\begin{aligned} n(2.45MeV) + p &\rightarrow\ n'(0keV - 2.45MeV) + p(0 - 2.45MeV) \\ n(2.45MeV) + D &\rightarrow\ n'(272keV - 2.45MeV) + D(0 - 2.18MeV) \\ n(2.45MeV) + {}^{12}C &\rightarrow\ n'(1.75MeV - 2.45MeV) + {}^{12}C(0 - 0.70MeV) \end{aligned} \tag{2}$$

The number ratio of scattered and primary neutrons is given by,

$$Y_{SN} / Y_{PN} = 1 - \exp(-\sigma / m_x \times \langle \rho_x R \rangle), \tag{3}$$

where m_x and $\langle \rho_x R \rangle$ are the mass and partial areal density of the specific target nucleus, and σ is the elastic scattering cross section. Assuming single elastic scattering in plasma, the spectrum of the downshifted neutrons can be derived from conservation of momentum and energy. For example, the neutron spectrum scattered by deuteron is,

$$\frac{dN(E_N)}{dE_N} = \begin{cases} if\ (-1 < \mu(E_N) < 1) \quad then \quad \dfrac{\rho_d R}{m_d} \dfrac{\pi (m_n + m_d)^2}{m_n m_d E_{PN}} \dfrac{d\sigma[E_{PN}, \mu(E_N)]}{d\omega} Y_{PN}, \\ otherwise \qquad\qquad 0, \end{cases} \tag{4}$$

$$where \qquad \mu(E_N) = \frac{E_N}{E_{PN}} \frac{(m_n + m_d)^2}{2 m_n m_d} - \frac{m_n^2 + m_d^2}{2 m_n m_d},$$

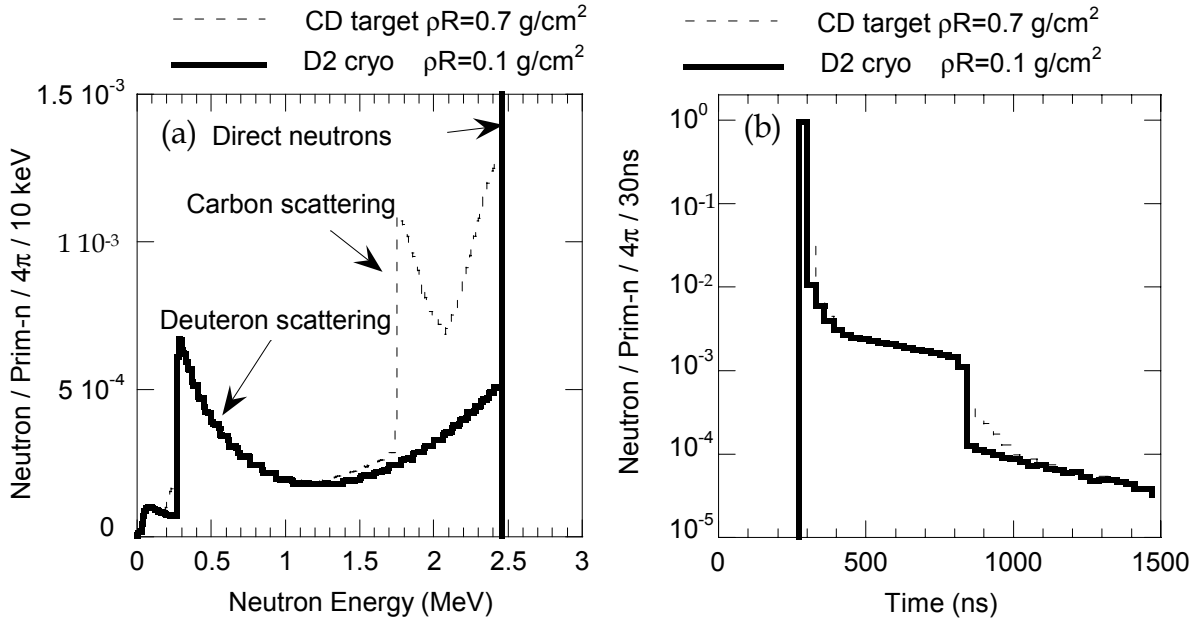

Fig. 1. (a) Spectrum of scattered neutron obtained by Monte Carlo simulation. The broken line and solid line is for the CD target (ρR = 0.7 g/cm^2) and D2 Cryo target (ρR = 0.1 g/cm^2), respectively. The spectrum below 1 MeV is almost identical for CD and D2 cryo target. The direct neutron spectrum is clipped. (b) The flight time spectrum for each target.

E_{PN} and E_N are energies of the primary neutron and the scattered neutron, m_n and m_d are the masses of the neutron and the deuteron, μ is the cosine of the neutron scattering angle in center of mass system, $\rho_d R$ is the partial areal density of deuteron in target plasma, $d\sigma/d\omega$ is the differential cross section of the neutron scattering, and Y_{PN} is the primary neutron yield. Neutron scattering by hydrogen and carbon can also be expressed in a similar way by substituting m_d with other target nuclei masses. More precise spectra including multiple scattering can be calculated with Monte Carlo simulations[1]. Fig. 1 (a) shows the scattered neutron spectra for deuterated plastic shell targets (ρR = 0.7 g/cm^2, broken line) and pure deuterium targets (D_2 cryo targets; ρR = 0.1 g/cm^2, solid line). The existence of carbon affects the spectrum only for energies above 1.75 MeV. The neutron spectra below 1 MeV are almost identical for CD and D_2 cryo target. This low energy tail (< 1 MeV) of the neutron spectrum is sensitive only to the deuterium partial areal density. Fig. 1 (b) shows the flight time spectrum at 600 cm from the target. The neutron scattering by heavier nuclei (in shell and hohlraum) does not cause distinct differences. That is why this technique is applicable to both direct and indirect drive target. The maximum areal density of down shifted neutron method is limited by the multiple neutron scattering inside the target. For the case of a deuterium cryo target, the limit is around $\rho_d R \sim 1.4$ g/cm^2 where 63% of primary neutrons are scattered.

2. INSTRUMENTATION

The principle of the downshifted neutron method is quite similar to the knock-on method[2]. Because of the long mean free paths of the neutrons, the downshifted neutron method is applicable to higher areal densities (up to 1.4 g/cm^2, for D_2 Cryo target). However, the experimental demonstration of the downshifted neutron method has never been reported. The yield of the downshifted neutrons is large (7% of primaries at $\rho_d R$ = 0.1 g/cm^2) compared to that of secondary neutrons produced by secondary t(d,n)α reactions in deuterium fuel plasma (up to 2% of primaries for ρR > 0.1 gm/cm^2 at an electron temperature of 1 keV)[3]. The difficulties of the downshifted neutron measurements by scintillator based time of flight spectroscopy are described as follows. (1) The energies of the downshifted neutrons are lower than the non-scattered primary neutrons (i.e. direct primaries). Detectors based on proton recoil (e. g. organic scintillator) yield smaller signal output for the downshifted neutrons. (2) Since they have quite broad energy spectra, the downshifted neutron signal is widely spread in time of flight. Therefore, the pulse height of the downshifted neutron signal is fainter

than for the direct primaries. (3) Prior to the downshifted neutrons, a large burst of direct primaries hits the detector. A long decay time fluorescence "after glow" caused by the direct primaries interferes with the detection of the weaker downshifted neutron signal, especially for current mode scintillation detectors.

These hurdles lead to corresponding detector requirements: (1) Sufficient output for low energy "single" neutrons. (2) Operated in counting mode, in order to detect the temporally spread signal as the temporally and/or spatially localized "single particle" signal. (3) Robust to the interference due to preceding strong burst of direct primaries. To achieve these requirements we propose a new detector concept. The detector is placed several meters away from the target and the direct primaries and downshifts are separated by time of flight (TOF). The scintillation signals are recorded by a gated image intensifier instead of a photo multiplier tube. The scintillation light caused by direct primaries is rejected by the image intensifier gate and the signal from downshifted neutrons is recorded as an image of bright spots.

In order to suppress the interference caused by the strong burst of direct primaries, we also adopt a multi-cell detector concept. The multi-cell detector utilizes a large number of identical TOF detectors[4]. Such a detector can increase the number ratio of detected downshifts to direct primaries in a single cell. Since the detection efficiency for a single cell is quite small, the number of primary neutron hits for a single cell is reduced to a few or less. The majority of cells detect no downshifts and some cells detect one downshift signal. For the cell that detects one downshifted neutron, the detected number ratio of downshifts to primaries is one to a few. Therefore, the multi-cell dramatically suppresses the interference caused by the direct primaries and all cells can recover before the arrival of downshifted neutron signal.

Fig. 2 shows the schematic of the instrumentation that we propose to achieve these requirements. The points of this instrumentation are as follows: (1) use a recently developed lithium glass scintillation fiber plate (LG-SCIFI) as a detector array, (2) couple the LG-SCIFI to a gated image intensifier and amplify the downshifted neutron signal in specific flight-time window of interest, (3) transfer the intensified image to a charge coupled device (CCD) that is protected against direct exposure to X rays, neutrons, and electromagnetic interference. The neutron signal is counted as the number of the bright spots in the gated image.

The advantages of an LG-SCIFI coupled with an image intensifier are: (1) The lithium glass has a high light output for low energy neutrons. Since $^{6}Li(n,t)\alpha$ is exothermic with Q = 4.8 MeV, the scintillator produces enough light even for low energy single neutrons; (2) Since the $^{6}Li(n,t)\alpha$ cross section has a large resonance on the low energy tail of downshifted neutron energy spectrum (Fig. 3), the lithium glass is more sensitive to downshifted neutrons and less sensitive to direct primaries; (3) Since $^{6}Li(n,t)\alpha$ is a prompt reaction and the scintillation decay time is relatively fast (~100 ns), the lithium glass is applicable for time gating operation. (4) The LG-SCIFI (40 mm diameters consist of 100-μm pixels) works as a 10^{5}-channel scintillator array. With a large number of individual channels, the number of detected primaries per channel decreases significantly while the downshifted detection is essentially binary.

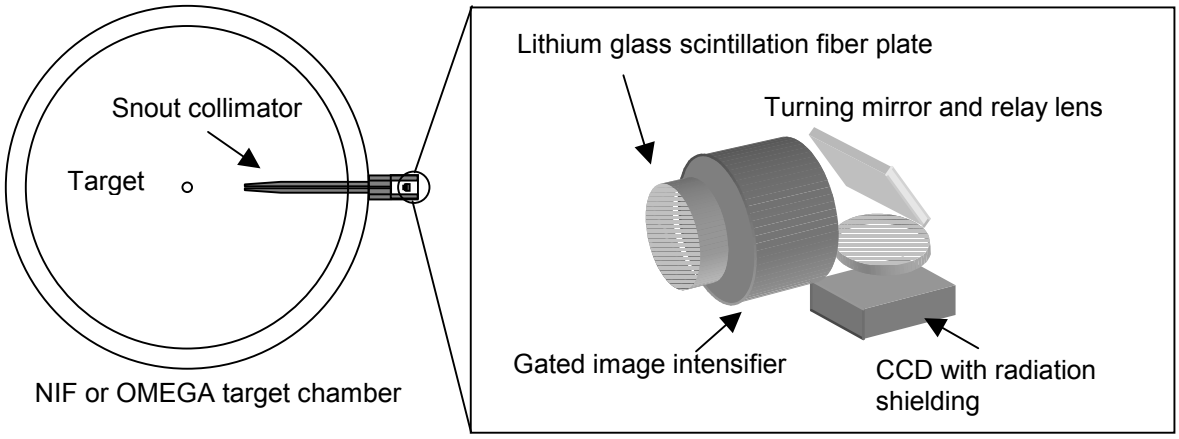

Fig. 2. Schematic of instrumentation of scattered neutron detection system.

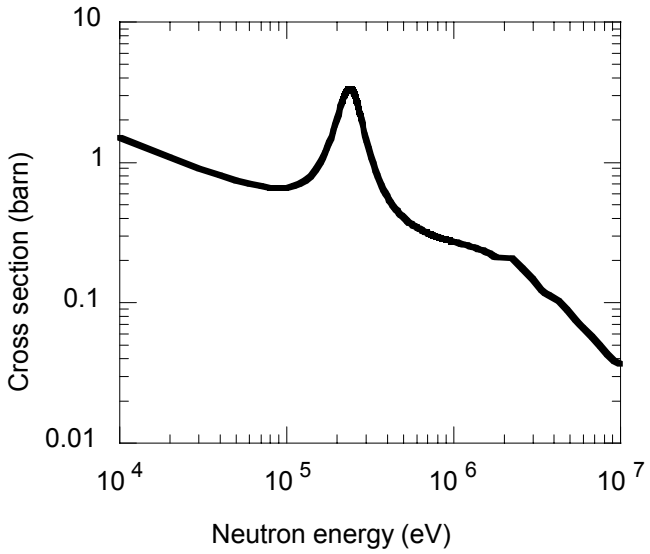

Fig. 3. Neutron cross section of ^{6}Li(n,t)α reaction from JENDL-3. The cross section has large resonance near the low energy tail of scattered neutron, e. g. 3.36 barn at 240 keV, 1.4 barn at 300 keV, and 0.2 barn at 2.45 MeV.

2.1 LITHIUM GLASS SCINTILLATION FIBER FACEPLATE

The LG-SCIFI detector is a slice of a scintillation-glass optical fiber bundle. One element of the scintillation optical fiber consists of a higher refractive index core made of scintillation-glass and cladding made of lower refractive index glass. This structure works as a stepped index optical fiber. A fraction of the scintillation light rays are trapped in the core region by total internal reflection on the core-clad interface and guided to the fiber ends. The LG-SCIFI detectors were originally developed for charged particle tracking in high-energy physics experiments[5]. The detector response to neutrons has also been investigated[6].

In the lithium glass, neutrons cause an exothermic reaction, ^{6}Li(n,t)α, with Q = 4.8 MeV. When the incident neutron energy is negligible compared to the Q value, the kinetic energies carried away by the reaction products are 2.05 MeV for the alpha and 2.73 MeV for the triton. These energetic charged particles excite the Ce^{3+} ions in the glass and cause scintillation. The stopping range of each particle in the glass is about 7μm for alphas and 40μm for tritons, respectively[7]. To avoid a loss of scintillation light due to escape of these particles from one cell, each fiber thickness should be several times larger than their stopping ranges. The absolute scintillation efficiency of the bulk scintillator is about 1.5% for electron excitation (e.g. NE905 reported in reference 7). It correspond to ~5 photons/keV. The absolute scintillation efficiencies for tritons and alphas are smaller than electron excitation. This is explained by "ionization quenching" caused by the higher specific energy loss for these ions. The total scintillation produced by an alpha (2.05 MeV) and a triton (2.73 MeV)is equivalent to an electron excitation of 1.5 MeV[7]. Therefore, about ~7500 photons are produced for a single ^{6}Li(n,t)α reaction in bulk glass scintillator.

One element of LI-SCIFI consists of a higher refractive index core and lower refractive index cladding material. Scintillation light rays that arrive at the core-clad interface with an angle of incidence larger than the critical angle for total reflection are trapped in the core and guided to the end of the fiber[8]. The trapping efficiency F can be estimated using the refractive index of core n_0 and clad n_1,

$$F = 0.5 \times (1 - {}^{n_1}\!/_{n_0}). \qquad (5)$$

When a typical scintillation glass n_0 = 1.55 is surrounded by cladding material of n_1 = 1.495, about 1.8% of scintillation light is trapped and guided to both ends of the fiber. With a reflective coating on the input edge of the fibers, the trapping efficiency can be improved, however the improvement is limited to less than a factor 2 due to light absorption and

scattering in the fiber. We are assuming that 3% of scintillation light is guided to the output edge of the fiber. Therefore, the light output for a single neutron capture event, Y_{SNC}, is ~225 photons. The residual scintillation light escapes from the fiber. Some of these photons enter and trap in adjacent fibers and cause cross talk. For better contrast of neutron-induced tracks, an extra mural absorber made of black glass should be applied to the outer surface of the cladding glass[5].

The scintillator time response is also one of the important requirements. The dead time of one scintillator element is decided by the decay time of scintillation. The neutron flight distance should be optimized so that the element hit by a direct neutron recovers before the arrival of the scattered neutron signal. A typical decay time of cerium doped lithium glass scintillator is 100 ns (90% - 10%)[9]. For the case of a 600cm neutron flight path, the flight time of direct primaries (2.45 MeV) is about 278 ns. When we observe scattered neutrons between 612 keV to 272 keV, the corresponding time window for the scattered neutron signal is from 556 to 833 ns (see Fig. 1 (b)). Thus the time interval from direct primaries to the beginning of the time window of downshifted neutrons is 278 ns. Therefore, the scintillation decay time is fast enough so that all scintillator elements can recover before arrival of the scattered neutron signal of interest.

The detection efficiency of the LG-SCIFI detector $\eta_{total}(E_n)$ is expressed by

$$\eta_{total}(E_n) = \frac{\Omega}{4\pi} \cdot \eta_{ff} \cdot \eta_i(E_n), \qquad (6)$$

where E_n is neutron energy, Ω is the solid angle subtended by LG-SCIFI, η_{ff} is the filling factor of the neutron sensitive region (core material) in the LG-SCIFI detector, and $\eta_i(E_n)$ is the intrinsic detection efficiency. Assuming that a LG_SCIFI of 4cm diameter is placed 600 cm away from the target, the geometric efficiency is $\Omega/4\pi = 2.78\times10^{-6}$. The expected filling factor of the sensitive volume in the LG-SCIFI detector is ~80%[10]. The intrinsic detection efficiency of the glass scintillator, η_i, can be approximated by,

$$\eta_i(E_n) = 1 - \exp\left(-n_{6Li}\sigma(E_n)t\right). \qquad (7)$$

where n_{6Li} is the number density of ^{6}Li, $\sigma(E_n)$ is the reaction cross section as a function of incident neutron energy, and t is the thickness of the detector. Lithium loaded glass scintillators with different lithium content (2.4 ~7.5 by weight) are available commercially. Scintillators loaded with enriched lithium in 95% ^{6}Li are also available. Typical glass scintillators like NE905 or GS20 (density 2.5 g/cm^2) contain 6.6% of lithium by weight. Therefore, n_{6Li} for typical glass is 1.56×10^{22}. When the scintillator thickness is 3cm, the intrinsic efficiency for direct primaries $\eta_i(2.45MeV)$ is 0.9 %. The intrinsic detection efficiency in the specific energy window of neutrons scattered by deuterons can be estimated by

$$\eta_{i,SN} = \frac{\int_{272keV}^{612keV} n_i(E_n)\frac{dN(E_n)}{dE_n}dE_n}{\int_{272keV}^{612keV}\frac{dN(E_n)}{dE_n}dE_n}, \qquad (8)$$

where $dN(E_n)/dE_n$ is the scattered neutron spectrum described in equation (1). For a 3-cm thickness detector, the intrinsic efficiency for this energy window is 3.2%. Since the ^{6}Li(n,t)α reaction has a large resonance at 240keV, the lithium glass scintillator is 3 times more sensitive to downshifted neutrons than to the direct primaries. This feature helps to reduce the interference by direct primaries. For example, when the primary neutron yield is 10^{11} and $\rho_d R = 0.1$ g/cm^2, the number of downshifted neutrons between 272 keV and 612 keV is 1.8×10^9, giving a number ratio of primary to downshifted neutrons of 50 to 1. However, due to the enhanced sensitivity of LG-SCIFI to lower energy neutrons, the ratio of detected primaries (1900) to detected downshifts (130) is only 15:1.

2.2 IMAGE INTENSIFIER

The LG-SCIFI is connected to the gated image intensifier for signal amplification and temporal gating. Because of its high spatial resolution (more than 20-line pairs/mm) and fast gating ability (10ns), we are planning to use a generation II proximity focus image intensifier. The generation II proximity image intensifier is a vacuum tube consisting of a photocathode, a micro channel plate (MCP), and a phosphor screen. The scintillation light is guided to the photocathode through an input window. Photoelectrons produced on the cathode are accelerated into the MCP. The electrons multiplied in the MCP are accelerated and re-converted to light on the phosphor screen. The sensitivity of the image

intensifier can be gated by instantly changing the cathode potential. When the photocathode potential is higher than the MCP input surface (~+30 V), electrons emitted from photocathode are repelled away from the MCP and signals are interrupted. When the photocathode potential is set lower than the MCP surface (~ -200V), photoelectrons are guided to the MCP and multiplied.

As an input window, a fiber optic faceplate is suitable to transfer the scintillation track image from the LG-SCIFI output to the photocathode. The fiber optic window contains 70% core glass (30% cladding), which gives 70% transmission. The light absorption at scintillation wavelengths may cause additional transmission loss in the fiber optic window.

For observation of scintillation light that has peak emission around 395 nm, a "bialkali" (K_2SbCs) photocathode is suitable. The timing response of gating operation is limited by the cathode capacity and resistivity. To obtain a fast response, a transparent electro-conductive nickel layer is required under the photo cathode material. This conductive layer absorbs ~30% of the input light. The intrinsic quantum efficiency of a general bialkali cathode at 395 nm can be up to 30%. However, taking into account the light absorption in the fiber optic window and the nickel conductive layer, the total quantum efficiency, $\eta_{cathode}$, for scintillation light is estimated to be 10%.

The photoelectrons emitted from the photocathode are amplified by the MCP. Using a double stage MCP with 1400V bias, an electron multiplication gain, G_{MCP}, of 1×10^4 can be obtained. After multiplication, electrons are accelerated to 6keV by an electric field applied between the MCP output surface and the phosphor screen. The phosphor material is selected to have a good matching to the spectral response of the CCD. A P46 ($Y_3A_{l5}O_{12}$: Ce) phosphor has maximum emission at 530nm and shows good matching. A typical quantum efficiency, $G_{phsphor}$, for P46 phosphor with 6keV electrons is 90 photons/electron. Accounting for the attenuation, efficiencies, and gain of the window, photo cathode, MCP and phosphor screen, the total image intensifier gain, G_{II}, is

$$\begin{aligned} G_{II} &= \eta_{cathode} \times G_{MCP} \times G_{phosphor} \\ &\sim 1 \times 10^5. \end{aligned} \qquad (9)$$

The image on the phosphor screen is transferred by a relay lens system. The magnification of the image transfer is 0.5 to keep the entire LG-SCIFI image on a 1" square CCD. The light coupling efficiency, η_{LC}, of the image relay lens system is determined by the solid angle subtended by the object lens:

$$\eta_{LC} = \frac{T}{16(L/D)^2}, \qquad (10)$$

where T is the lens transmission, L and D are the working distance and the aperture diameter of object lens, respectively. Assuming T=0.9, and L/D = 2.5, the light collection efficiency is 0.9%.

Therefore, the number of photons incident on the CCD for a single neutron capture event is,

$$\begin{aligned} N &= Y_{SNC} \times G_{II} \times \eta_{LC} \\ &= 2 \times 10^5. \end{aligned} \qquad (11)$$

An image of a 100-μm-scintillator core is transferred to the CCD as a 50-μm square image. Taking into account the finite spatial resolution of the system, the signal photons are spread over ~4-9 25μm CCD pixels. The signal intensity for one pixel is at least ~2×10^4 photons per pixel and it is well above the noise level of the CCD.

If the CCD noise due to background ionizing radiation (stray neutrons and gamma ray induced by neutrons) is not significant, the shielding of the CCD is not crucial and it is possible to use a fiber optic image reducer for coupling between the image intensifier and the CCD. Since the coupling efficiency of a fiber optic image reducer is one order larger than that of a relay lens system, the required gain of the image intensifier is reduced to 10^4 and an image intensifier with a single MCP can be used instead of double MCP.

3. BACKGROUND ESTIMATION

The most critical issue of this scheme is collimation. Almost all the direct primaries impinge on the target chamber wall, other diagnostics, or structures near the detector. These direct primaries are scattered by these structures and the detector is exposed to a finite fraction of them. These "non-target scattering" neutrons are both downshifted in energy and take a longer flight path to the detector. Therefore, some parts of them hit the detector in the temporal window of the downshifted neutron signal and make background counts. Since these neutrons impinge on the detector from outside of the direct view cone, it is possible to reduce these backgrounds using a cone shaped collimator. A neutron shielding enclosure, which covers all solid angles around the detector except for the target view, also works well to reduce the background neutrons from the side and behind the detector.

In addition, the neutron scatterings inside the shielding enclosure also make background counts. The direct neutrons, which outnumber the downshifted neutron signal 50 to 1, arrive at the detector prior to the downshifted neutron signal and are scattered by the detector itself. Then these neutrons are scattered several times in the enclosure walls and make a "fog" of moderate energy (below 100 keV) stray neutrons. Since the lithium glass scintillator is sensitive to moderate energy neutrons, these stray neutrons cause background counts. In order to reduce this effect, the shielding must enclose enough space around the detector. The inner walls of the enclosure reflect the stray neutrons and a finite fraction of them hit the detector. The increased standoff distance reduces the probability of that a neutron scattered off the shielding will return and hit the detector. In other words, all the stray neutrons are captured in the collimator wall surface or detector in the long run. If the enclosure room is large enough, the surface volume of the enclosure inner walls is larger than the scintillator volume and almost all the stray neutrons are captured in the enclosure walls.

Material selection of the shielding enclosure is also important for background reduction. When stray neutrons are captured by hydrogen in the collimator material, 2.223 MeV γrays are produced by p(n, γ)d reactions. These γ rays also cause background. To suppress this, a polyethylene mixed with Li_2CO_3 works well[11]. Natural lithium contains 7.5% ^{6}Li and it captures stray neutron by the ^{6}Li(n,α)t reaction without γ ray production. The efficiency of neutron capture is decided by the number density of target nuclei and the capture cross section. When the abundance of Li_2CO_3 is 35% by weight, the neutron capture efficiency of ^{6}Li is 20 times larger than hydrogen and the γ ray is suppressed down to 5%.

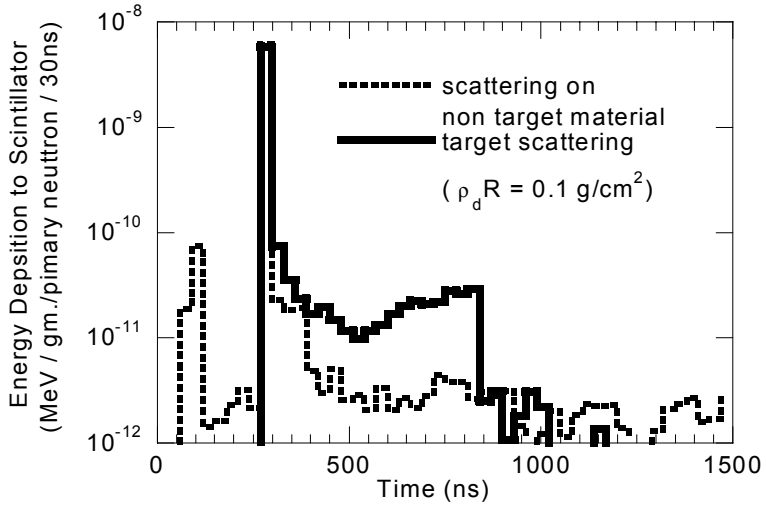

Fig. 4. Estimation of background by Monte Carlo calculation. The vertical scale indicates energy deposition to the detector by the neutrons and photons. The dashed line shows the primaries and that scattered by non-target material (background). The solid line shows primaries and downshift signal. Factor 7 of signal to background ratio is expected for ρR = 0.1 g/cm^2.

Fig. 4 shows the result of background estimation with MCNP[1]. The vertical scale indicates the energy deposition to the detector by neutrons and neutron-induced γ-rays. The effect of the Q value of the nuclear reactions in the scintillator is included in the energy deposition. The dashed line shows the background due to neutron scattering on "non-target material". The calculation includes the neutron scattering on the vacuum chamber, collimators, and the detector itself. The solid line shows the signal level obtained by the model with "target scattering only". With the collimator design, the signal to background ratio of 7 can be achieved for $\rho_d R = 0.1$ g/cm^2.

4. SUMMARY

We proposed a new method for areal density measurement based on down shifted neutron counting. For deuterium filled fuel, the neutron spectrum below 2.45 MeV is sensitive to the areal densities of specific light nuclei in the imploded plasma. In order to observe these lower energy neutron signals, the detector should have large output for single particle detection and should be robust to interference from 2.45 MeV direct primaries. We propose to use a LG SCIFI detector for the downshifted neutron counting. The LG-SCIFI yields ~ 225-photons for single neutron detection. With amplification using a gated image intensifier, these single neutron events are observable by a CCD. The detection efficiency of LG-SCIFI for a downshifted neutron is 3%, which is 3 times more efficient than for 2.45 MeV direct primaries. A collimator can reject the background due to neutron scattering on the target chamber and other structures. The background produced in the collimator can also be suppressed by a suitable design of the collimator shape and material selection.

ACKNOWLEDGEMENTS

This work was performed under the auspices of the U.S. Department of Energy by the University of California, Lawrence Livermore National Laboratory under contract No. W-7405-Eng-48.

REFERENCES

1. J. F. Briesmeister, Ed., *MCNP – A General Monte Carlo N-Particle Transport Code, Version 4C*, Report No. LA-13709-M, Los Alamos National Laboratory, 2000.
2. S. Kacenjar, L.M. Goldman, A. Entenberg, and S. Skupsky, "<ρR> measurement in laser-produced implosions using elastically scattered ions", *J. Appl. Phys*. **56,** pp. 2027-2032, 1984.
3. H. Azechi, M. D. Cable, and R. O. Stapf, "Review of secondary and tertiary reactions, and neutron scattering as diagnostic techniques for inertial confinement fusion targets", *Laser and Particle Beams* **9,** pp.119-134, 1991.
4. S. M. Lane, M. D. Cable, W. R. Graves, R. A. Lerche, D. R. Slaughter, C. L. Wang, S. G. Prussin*, Lawrence Livermore National Laboratory Report*, No. UCRL-50021-84, pp.5-61 to 5-64, Lawrence Livermore National Laboratoy, 1985.
5. M. Atkinson, J. Fent, C. Fisher, P. Freund, et al., "Initial tests of a high resolution scintillating fibre (SCIFI) tracker," *Nucl. Instr. Meth. A* **254**, pp. 500-514, 1987.
6. P. L. Reeder, A. J. Peurrung, W. C. Richey, H. H. Chen-Mayer, et al., "Imaging neutron beams with scintillating fiber faceplates", *Nucl. Instr. Meth. A* **402,** pp. 155-163, 1998; P. Ottonello, V. Palestini, G. A. Rottigni, G. Zanella, R. Zannoni, "Slow neutron beam diagnostics with a scintillating fiber detector", *Nucl. Instr. Meth. A* **366**, pp. 248-253, 1995; K. H. Abel, R. J. Arthur, M. Bliss, D. W. Brite, *et al.*, "Scintillating-glass-fiber neutron sensors", *Nucl. Instr. Meth. A* **353,** pp. 114-117, 1994; P. Ottonello, G.A. Rottigni, G Zanella, R. Zannoni, "Slow neutron imaging using scintillating glass optical fibers", *Nucl. Instr. Meth. A* **349**, pp. 526-531, 1994.
7. A. W. Dalton, "Light conversion efficiency of small lithium scintillators for electrons protons, deuterons and alpha particles", *Nucl. Instr. Meth. A* **254**, pp. 361-366, 1987.
8. Glenn F Knoll, *Radiation Detection and Measurement third edition,* p. 256, John Wiley & Sons, New York, 1999.
9. E. J. Fairley and A. R. Spowart, "Neutron scintillating glasses part III pulse decay time measurements at room temperature" *Nucl. Instr. Meth* **150**, pp. 159-163, 1978.
10. P. Ottonello, G.A. Rottigni, G Zanella, R. Zannoni, "Slow neutron imaging using scintillating glass optical fibers", *Nucl. Instr. Meth. A* **349,** pp. 526-531, 1994.
11. P. Batistoni, B. Esposito, M. Martone, and S. Mantovani, "Design of the neutron multicollimator for Frascati tokamak upgrade", *Rev. Sci. Instrum*. **66**, pp. 4929-4957, 1995.